Microsecond Deprotonation of Aspartic Acid and Response of the α/β Subdomain Precede C-Terminal Signaling in the Blue Light Sensor Plant Cryptochrome

ARTICLE *in* JOURNAL OF THE AMERICAN CHEMICAL SOCIETY · APRIL 2015

Impact Factor: 12.11 · DOI: 10.1021/jacs.5b01404 · Source: PubMed

3 AUTHORS, INCLUDING:

Tilman Kottke

Bielefeld University

35 PUBLICATIONS **897** CITATIONS

SEE PROFILE

JACS
JOURNAL OF THE AMERICAN CHEMICAL SOCIETY

Article

pubs.acs.org/JACS

Microsecond Deprotonation of Aspartic Acid and Response of the α/β Subdomain Precede C-Terminal Signaling in the Blue Light Sensor Plant Cryptochrome

Christian Thöing, Sabine Oldemeyer, and Tilman Kottke*

Physical and Biophysical Chemistry, Department of Chemistry, Bielefeld University, Universitätsstraße 25, 33615 Bielefeld, Germany

Supporting Information

ABSTRACT: Plant cryptochromes are photosensory receptors that regulate various central aspects of plant growth and development. These receptors consist of a photolyase homology region (PHR) carrying the oxidized flavin adenine dinucleotide (FAD) cofactor, and a cryptochrome C-terminal extension (CCT), which is essential for signaling. Absorption of blue/UVA light leads to formation of the FAD neutral radical as the likely signaling state, and ultimately activates the CCT. Little is known about the signal transfer from the flavin to the CCT. Here, we investigated the photoreaction of the PHR by time-resolved step-scan FT-IR spectroscopy complemented by UV−vis spectroscopy. The first spectrum at 500 ns shows major contributions from the FAD anion radical, which is demonstrated to then be protonated by aspartic acid 396 to the neutral radical within 3.5 μs. The analysis revealed the existence of three intermediates characterized by changes in secondary structure. A marked loss of β-sheet structure is observed in the second intermediate evolving with a time constant of 500 μs. This change is accompanied by a conversion of a tyrosine residue, which is identified as the formation of a tyrosine radical in the UV−vis. The only β-sheet in the PHR is located within the α/β subdomain, ~25 Å away from the flavin. This subdomain has been previously attributed a role as a putative antenna binding site, but is now suggested to have evolved to a component in the signaling of plant cryptochromes by mediating the interaction with the CCT.

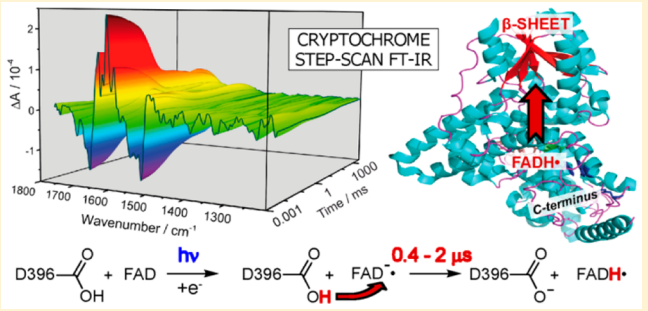

INTRODUCTION

Cryptochromes have been recognized as ubiquitous flavoproteins with a wide variety of functions and mechanisms in all kingdoms of life.[1] They exhibit homology to the photolyases, flavoproteins that repair DNA upon UVA light exposure.[2] Structurally, they all share a similar N-terminal photoactive domain of ~500 amino acids, the photolyase homology region (PHR). The PHR consists of an α/β subdomain, which may bind an antenna chromophore, as well as an α-helical subdomain, which noncovalently binds a flavin adenine dinucleotide (FAD) as a cofactor. Most cryptochromes possess an additional C-terminal extension (CCT), which is poorly conserved and highly variable in sequence and length. The CCT has been shown to be essential and sufficient for signal transduction in the plant *Arabidopsis*,[3] more precisely an 80-amino acid stretch comprising also some residues of the PHR C-terminus.[4]

The most prominent role of cryptochromes from a historical perspective is their function as blue light receptors.[5] As such they regulate central aspects of growth and development in plants,[6] and are involved in the light-dependent entrainment of the circadian clock in plants[7] and insects.[8] Moreover, cryptochromes alter gene expression upon light induction in diatoms,[9] green algae,[10] and bacteria.[11] In contrast, some cryptochromes found in insects[12] and mammals,[13] including humans, act as light-*irresponsive* components of the circadian clock. Cryptochromes have been shown to mediate light-dependent magnetosensitivity in fruit flies,[14] a property that has been demonstrated in vitro on plant cryptochromes.[15] These findings have fueled initial proposals that cryptochromes serve as magnetoreceptors in the magnetic compass of migratory birds.[16]

The photoreactions of cryptochromes have turned out to be rather complex and diverse, exhibiting different reaction pathways of the flavin chromophore and involving several amino acids in electron transfer and proton transfer reactions. In plant cryptochromes, absorption of blue light induces the conversion of the oxidized FAD (FAD_{ox}) into the neutral radical ($FADH^{\bullet}$), which likely acts as the signaling state in vivo (Figure 1).[17−19] Time-resolved UV−vis spectroscopy on cryptochrome 1 from *Arabidopsis* (*At*Cry1) and on CPH1 (*Chlamydomonas* photolyase homologue 1) from the green alga *Chlamydomonas reinhardtii* has demonstrated that the flavin is rapidly reduced to the anion radical ($FAD^{\bullet-}$) by a nearby tryptophan residue,[15,20] which is part of a highly conserved tryptophan triad.[21] The ultrafast Trp → FAD and Trp → Trp electron transfer reactions have been determined to proceed

Received: February 8, 2015
Published: April 24, 2015

DOI: 10.1021/jacs.5b01404
J. Am. Chem. Soc. 2015, 137, 5990−5999

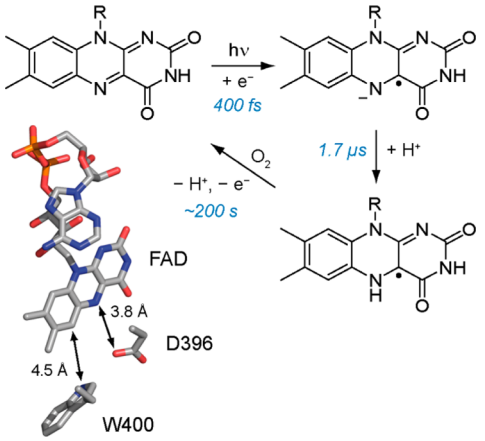

Figure 1. Photoreaction of the chromophore flavin adenine dinucleotide (FAD) in plant cryptochromes. The structure on the left represents a section from the flavin binding pocket in *Arabidopsis* cryptochrome 1 (*At*Cry1) (PDB code: 1U3C). After light absorption by oxidized FAD, the anion radical $FAD^{\bullet-}$ is formed via an ultrafast electron transfer. A microsecond proton transfer to the flavin then yields the neutral radical $FADH^{\bullet}$, which likely acts as the signaling state in vivo. The tryptophan W400 and the aspartic acid D396 are located close to the flavin, and therefore are considered as likely candidates for the electron and the proton donor, respectively. The FAD is reoxidized by oxygen within minutes.

with time constants of 0.4 and 31 ps, respectively.[22] The terminal tryptophan cation radical is stabilized by a biphasic proton transfer to the nearest environment within 100 ps and 500 ns[22,23] and then decays into a tyrosine radical within a few milliseconds.[21] The fate of $FAD^{\bullet-}$ seems to be detached from the processes within the tryptophan triad, because its protonation was reported to occur on a time scale of a few microseconds[15,20] and is thus delayed by 6–7 orders of magnitude with respect to the initial electron transfer. This distinct separation of both processes appears paradox, given that the proton donor D396 (D393 in CPH1), as identified by infrared spectroscopy,[24−26] is located in close proximity to the flavin in the crystal structure of *At*Cry1-PHR (Figure 1).[27] However, a structural rearrangement of D396 may be prerequisite for the proton transfer, because it forms a hydrogen bond to an oxygen atom of the protein backbone.

It should be noted that this reaction model is not unanimously accepted. First, in vivo experiments on mutants in the tryptophan triad of *At*Cry2 have cast doubt on the biological significance of the triad for the flavin photoreduction and consequently on the role of the oxidized state of flavin as the dark form.[28] This discrepancy might be reconciled by the recent finding that the binding of nucleotides to *At*Cry2 in vivo opens up alternative electron transfer pathways.[29] Second, the sequence and time scales of the processes have been questioned by theoretical studies that predicted an ultrafast proton transfer from D396 to flavin.[30,31] Recent experiments suggest that the latter process exists as a competing pathway, which can be suppressed by binding of ATP, thereby significantly increasing the yield of the reaction.[23] However, direct evidence on the protonation status of D396 by time-resolved spectroscopy is lacking.

While there has been significant progress in the investigation of the chemical photoreduction pathways, little is known about the resulting changes in the secondary and tertiary structure of plant cryptochromes. These changes, however, may play a crucial role for the initiation of signaling processes. Fourier transform infrared (FT-IR) spectroscopy has provided evidence for a light-induced change in turn elements within the PHR.[25] Furthermore, transient grating spectroscopy revealed a large decrease in the diffusion coefficient of the protein with a time constant of 0.4 s after excitation, which was interpreted as a partial unfolding of the CCT.[32] This region of *At*Cry1 has been shown to be particularly sensitive to light-dependent trypsin digestion.[33] It contains a linear motif that may bind for inhibition to the E3 ubiquitin ligase COP1 (constitutive morphogenesis 1) after the release of the CCT from the PHR.[33]

Therefore, we set out to probe conformational changes preceding the C-terminal unfolding by time-resolved FT-IR difference spectroscopy on the PHR of the plant cryptochrome CPH1 in the time range from submicroseconds to seconds. The FT-IR technique has proven to be a valuable tool for identifying changes in the chromophore, single amino acids, and secondary structure of proteins.[34] The time-resolved step-scan and rapid-scan FT-IR techniques have been used to access the submicrosecond to millisecond and millisecond to minute time ranges, respectively.[35] In the difference mode, only those contributions are resolved that change in the reaction under investigation. Vibrational modes of secondary structure elements are analyzed in the amide I (1620–1695 cm^{-1}) and amide II (1520–1590 cm^{-1}) regions,[34,36] which contain coupled modes originating from the amide bonds. The combinations of signals of both types clearly correlate with certain secondary structure elements in statistical analyses.[36]

To date, the only steady-state infrared difference experiments on plant cryptochromes have been performed on *At*Cry1[26] and CPH1-PHR.[24,25] In the present time-resolved FT-IR study, we identified the presence of $FAD^{\bullet-}$ at 500 ns after the laser pulse and monitored its protonation by aspartic acid 396 with a time constant of 0.4–2 μs (*At*Cry1 numbering is used here and below for clarity). Furthermore, we detected a change in β-sheet structure in the late microsecond time range and assigned it to the α/β subdomain of CPH1-PHR. As we will deduce in the following, this change may play an important role in the initiation of the signal transduction in plant cryptochromes.

EXPERIMENTAL SECTION

Sample Preparation. The PHR domain of CPH1 was expressed in *E. coli* and purified via Strep-Tactin affinity chromatography as described previously.[37] For cell lysis, purification, and dialysis, a 50 mM sodium phosphate buffer, pH 7.8, containing 20% (v/v) glycerol and 100 mM NaCl was used. For time-resolved UV–vis spectroscopy, the concentration of the sample was adjusted to reach OD_{450} = 0.3. For FT-IR spectroscopy, the protein was washed 3 times with 20 mM sodium phosphate buffer, pH 7.8, 100 mM NaCl, 1% (v/v) glycerol and concentrated to an OD_{450} >10 by ultrafiltration using Vivaspin 500 filter devices (Sartorius Stedim Biotech) with 50 kDa cutoff. Samples were shock frozen and stored at −80 °C. Potassium ferricyanide was added to the sample solution to reach a final concentration of 10 mM. A droplet of 2 μL was placed on a CaF_2 window (20 mm diameter). It was kept at 20 °C and atmospheric pressure for up to 2 min to gently reduce the water content and then sealed with a second window. Thus, we obtained a well-hydrated film with an absorbance ratio of amide I/water (1650 cm^{-1}) to amide II (1550 cm^{-1}) of 2.3–2.5.

FT-IR Spectroscopy. All FT-IR experiments were conducted using an IFS 66v spectrometer (Bruker) equipped with a photoconductive mercury cadmium telluride (MCT) detector at a spectral resolution of 4.5 cm^{-1}. An infrared band-pass filter (Laser Components) was used to restrict the spectral range to 1974–988 cm^{-1} and to block stray light. For excitation, a 450 nm light pulse with 10 ns duration and 16–

DOI: 10.1021/jacs.5b01404
J. Am. Chem. Soc. 2015, 137, 5990–5999

19 mJ energy was generated by a tunable optical parametric oscillator system (Opta), which was pumped by the 355 nm third harmonic of a Nd:YAG laser (Quanta-Ray GCR-12, Spectra Physics). Single laser pulses were selected from the 10-Hz repetition rate by an optical shutter (LSTXY, nm Laser Products). The temperature of the sample was kept constant at 10 °C by a circulating water bath.

For the step-scan experiments, 449 mirror positions were recorded with two coadditions at an excitation rate of 0.25 Hz. 1000 equidistant time slices of 5 μs were sampled up to 5 ms at each mirror position. In the time range −129 to −4 μs before the emission of the laser pulse, 25 dark spectra were recorded, averaged, and used for calculating the light-induced difference spectra. Each protein sample was used for up to five step-scan experiments, corresponding to ∼4500 excitations per sample. The stability of the protein for this number of excitations was checked by rapid-scan experiments with the same excitation rate. For the first spectrum at 0.5 μs (−4 to 1 μs), 258 coadditions with a strong 1545 cm^{-1} flavin band were selected and averaged. The resulting spectrum was scaled in intensity by a factor of 3, which was calculated by extrapolating the global fit of the 1354 cm^{-1} band to 0.5 μs. A scaling factor of 5 would be expected theoretically because the illuminated state was recorded only for 1 μs in the first 5 μs time window. The deviation is attributed to the short integration time, which may lead to some nonlinearities in the absolute band intensities. For the spectra beginning at 3.5 μs, 246 coadditions were selected, in which the amide I region could be resolved. Except where explicitly stated otherwise, spectra of intermediates were scaled with respect to the band of oxidized flavin near 1354 cm^{-1}, which does not overlap with amide I/II bands and has been found not to be compensated by contributions from the product states.[38]

The rapid-scan experiments were performed with a mirror velocity of 150 kHz in a splitted single sided, forward−backward mode. To overcome a general inaccuracy of ±30 ms in the timing because of the independence in frequency of interferometer mirror (10.52 Hz) and laser (10 Hz), synchronization was achieved by integrating a 10 ms TTL pulse from the spectrometer signaling the readiness for measuring an interferogram and a 2.2 ms TTL pulse from the laser after emission in a home-built electronic device. An output TTL pulse was only generated if both incoming pulses overlapped for ≥10 μs. TTL pulses were generated before each experiment to renew the synchronization between spectrometer and laser, which was confirmed by a simulation (see Supporting Information). The first spectrum was recorded from (4.3 ± 1.2) ms to (40.2 ± 1.2) ms with a midpoint of (22.3 ± 1.7 ms) after the laser pulse, and further 81 spectra were recorded until 3.883 s. The excitation rate was 0.17 Hz. For each rapid-scan experiment, 512 cycles were performed and averaged afterward. 38 data sets were selected and averaged, resulting in 19 456 scans per spectrum.

Data Analysis. The time-resolved spectra were analyzed with MATLAB (The Mathworks). Step-scan data recorded after 126 μs and rapid-scan data taken after 330 ms were summarized on a logarithmic time scale to increase the signal-to-noise ratio. Contributions of the broad water band at around 1650 cm^{-1} were subtracted from the individual spectra (see Supporting Information). For the kinetic analysis, the step-scan data (3.5 μs-4.62 ms) and rapid-scan data (22.3 ms-3.63 s) were concatenated (matrix $\boldsymbol{A}$). A weighted global fit was applied with weighting factors calculated from the variance along the wavenumber dimension and using a kinetic model of sequential first-order reactions with four intermediates. A fit with fewer intermediates did not fully account for all significant spectral differences within the data set, whereas a fit with more intermediates yielded pairs of similar lifetimes. To account for an observed decrease in the yield in the sequence of intermediates, the kinetic model was extended by back reactions from intermediates to the dark state (see Supporting Information). The nonlinear fits were performed with the program SolvOpt for MATLAB. The concentration profiles $\boldsymbol{C}$ resulting from the global fits were used to calculate the SADS $\boldsymbol{D}$ via matrix division according to $\boldsymbol{D} = \boldsymbol{A}\boldsymbol{C}^{+}$ (with $\boldsymbol{C}^{+}$ being the pseudoinverse of $\boldsymbol{C}$). Further kinetic analysis was performed with OriginPro 9.1 (OriginLab).

UV−Vis Spectroscopy. The experimental setup for time-resolved UV−vis difference spectroscopy has been described previously.[39] For excitation, 450 nm light pulses were generated by the laser system described above with an energy density of 2 mJ/cm^2 at the sample at a rate of $(1.6\ s)^{-1}$. The setup was further improved for the study of slowly recovering systems. Multiple excitations were minimized by using a magnetic stirrer driving a 5 mm stirring bar inside the 10 × 10 mm cuvette for 750 ms after each detection. A horizontal geometry of the excitation beam with 4 × 10 mm (height × width) ensured a fast sample exchange within a total volume of 2 mL. A mirror was placed behind the exit window to obtain a homogeneous excitation. The opening time of the probe light shutter was set to 200 μs or 1 ms depending on the measuring time window. By alternating the recording of reference and signal spectra, contributions from previous excitations were avoided. All experiments were conducted at 20 °C. The integration time was set to 10, 100, and 500 μs for difference spectra recorded at 17 μs, 0.3−1.5 ms, and 5−5000 ms, respectively. Each spectrum of CPH1-PHR was obtained by averaging 6−39 separate experiments, in which each sample was excited 3 times. Additionally, difference spectra of $FADH^{\bullet}$ in CPH1-PHR and $TyrO^{\bullet}$ in water were recorded as a reference (see Supporting Information). The kinetics of $Trp^{\bullet}$ and $TyrO^{\bullet}$ in CPH1-PHR were analyzed by a simultaneous fit on the basis of the reaction scheme $Trp^{\bullet} \rightarrow TyrO^{\bullet} \rightarrow$ TyrOH. Accordingly, $[Trp^{\bullet}]$ was fitted by the rate law $y = y_0 + A_0 \exp(-k_1 t)$ and $[TyrO^{\bullet}]$ by the rate law $y = y_0 + A_0((k_1)/(k_2 - k_1))(\exp(-k_1 t) - \exp(-k_2 t))$, with k_1, k_2 as rate constants, A_0 as the initial $Trp^{\bullet}$ concentration, and y_0 as the residual concentration. The fit was performed with shared parameters k_1 and A_0.

RESULTS

Decay of FAD Anion Radical in Plant Cryptochrome. The first measurement window by time-resolved infrared spectroscopy on CPH1-PHR monitored processes up to 1 μs after the laser pulse. The lifetime of $FAD^{\bullet-}$ had previously been determined to 1.7 μs by UV−vis spectroscopy.[20] Therefore, the resulting spectrum at 500 ns was directly compared with the steady-state light-*minus*-dark difference spectrum of $FAD^{\bullet-}$ (Figure 2A), which had been generated in the D396C mutant of CPH1 by blocking the proton transfer to the FAD.[24] Negative bands in the difference spectra originate from the dark state. Both spectra exhibit the characteristic signature of oxidized flavin with bands at 1577, 1547, and 1354 cm^{-1}, which are typically found in difference spectra of flavoproteins.[26,40,41] The carbonyl bands of the C(4)=O group[25] at 1708 and 1692 cm^{-1} are not resolved in the 500 ns spectrum of the wild type, but show up as a broad contribution at ∼1698 cm^{-1}. Additionally, a band at 1672 cm^{-1} is found in the time-resolved spectrum, which is assigned to the C(2)=O group.[25]

Positive bands in the difference spectra represent the state formed directly after illumination. In the spectrum of the D396C mutant, the bands at 1655, 1626, 1518, and 1490 cm^{-1} are considered as marker bands of $FAD^{\bullet-}$.[24,42] In comparison, the 500 ns spectrum features essentially the same band pattern at these positions, the difference being that the carbonyl bands at 1655 and 1626 cm^{-1} are slightly downshifted by 4−5 cm^{-1}. This difference can be explained by the presence of a cysteine instead of the aspartic acid at position 396 of the mutant and thus an altered environment in the flavin binding pocket. It is concluded that the 500 ns spectrum of the wild type contains the major contribution from $FAD^{\bullet-}$.

In addition to the marker bands of $FAD^{\bullet-}$, the 500 ns spectrum shows some difference bands at positions similar to those in the later spectra (t > 8.5 μs), in which $FAD^{\bullet-}$ completely decayed into $FADH^{\bullet}$. These bands can therefore be assigned to the formation of $FADH^{\bullet}$. The pronounced positive band at 1641 cm^{-1} is a marker band of $FADH^{\bullet}$ in CPH1-PHR.[25] The negative bands at 1405, 1354, and 1251

DOI: 10.1021/jacs.5b01404
J. Am. Chem. Soc. 2015, 137, 5990−5999

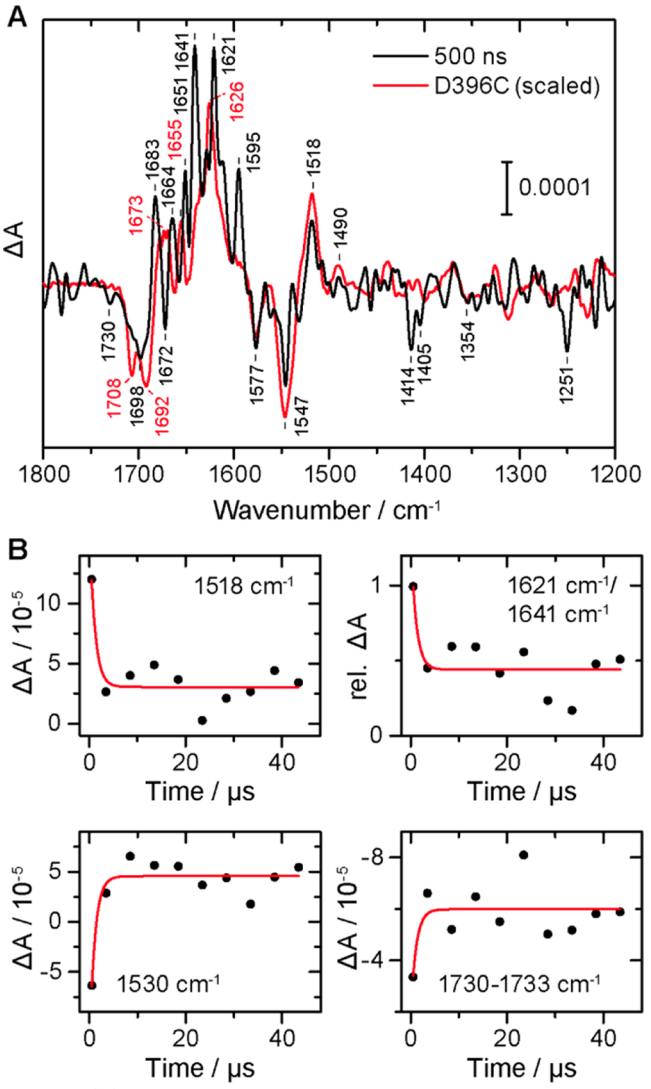

Figure 2. (A) Light-induced FT-IR difference spectrum of the PHR of the plant cryptochrome CPH1 recorded 500 ns after the laser pulse. For comparison, the steady-state difference spectrum of the D396C mutant is depicted, which forms $FAD^{\bullet-}$ upon illumination (taken from ref 24). The flavin band near 1354 cm^{-1} was used for scaling. (B) Simultaneous monoexponential fit of the marker bands for the decay of $FAD^{\bullet-}$ (top) and for the formation of $FADH^{\bullet}$ (bottom). The ratio $\Delta A_{1621}/\Delta A_{1641}$ was plotted, because both $FAD^{\bullet-}$ and $FADH^{\bullet}$ contribute to the absorption at 1621 cm^{-1}. The band at 1730−1733 cm^{-1} can be attributed to the deprotonation of the aspartic acid D396. The ΔA axis was inverted to demonstrate that this deprotonation occurs concomitantly with the formation of $FADH^{\bullet}$.

cm^{-1} originate from oxidized flavin and have been observed in difference spectra of other flavoproteins as well,[26,40,41] whereas the assignment of the 1414 cm^{-1} band to FAD_{ox} remains tentative. Similarly, a small but significant negative band at 1730 cm^{-1} is observed in the 500 ns spectrum of the wild type but not in the spectrum of the mutant, indicating a partial deprotonation of the aspartic acid D396.[24,25]

To obtain the lifetime of the $FAD^{\bullet-}$ protonation, the difference absorbance of the marker band of $FAD^{\bullet-}$ at 1518 cm^{-1} as well as those of $FADH^{\bullet}$ at 1530 cm^{-1} and of the aspartic acid at 1730−1733 cm^{-1} were analyzed for the first 10 spectra after the laser pulse (0.5−43.5 μs) (Figure 2B). Additionally, the ratio between ΔA_{1621} and ΔA_{1641} was determined as an indicator for the relative concentration of $FAD^{\bullet-}$ and $FADH^{\bullet}$, because both exhibit a band at 1622−1625 cm^{-1}.[24,25] A simultaneous monoexponential fit of all four band kinetics yielded a lifetime of (1.1 ± 0.7) μs. The significance of this value is lowered by the lack of time points in the early microsecond time region. Nonetheless, lower and upper limiting values for the lifetime of τ = 0.4 μs and τ = 2 μs, respectively, can be given. A faster decay of $FAD^{\bullet-}$ would render its detection as the major species at 500 ns practically impossible (Figure S1, Supporting Information), whereas a slower decay of $FAD^{\bullet-}$ would lead to a detectable contribution of $FAD^{\bullet-}$ to the second spectrum at 3.5 μs (>22% of the signal at 500 ns). These considerations lead to a more substantiated range for the lifetime of 0.4 $\mu s < \tau < 2$ μs, which is in sufficient agreement with the reported lifetime for $FAD^{\bullet-}$ of 1.7 μs.[20] As illustrated by the kinetics of the band at 1730−1733 cm^{-1}, D396 is completely deprotonated within 3.5 μs after illumination.

In addition to the flavin-specific bands, the spectrum of the D396C mutant also contains a band at 1673 cm^{-1}, which has been attributed to a light-induced change in turn elements in the wild type.[25] The 500 ns spectrum of the wild type contains two bands at 1683 and 1664 cm^{-1} in this region, separated by the negative carbonyl band of FAD_{ox} at 1672 cm^{-1}. The origin of these bands remains unclear. It may be speculated that they function as precursors of the amide I band at 1667−1671 cm^{-1} in the later spectra.

In summary, the spectral features resolved in the spectra of the wild type imply that the anion radical is present to a major extent at 500 ns. The kinetics of selected marker bands allowed for an approximate determination of the $FAD^{\bullet-}$ lifetime to 0.4−2 μs. Within the same time window, deprotonation of the proton donor D396 was detected.

Changes in Conformation upon and after Formation of the FAD Neutral Radical. We obtained a data set covering a continuous range of more than 6 orders of magnitude in time by including step-scan experiments from 0 μs to 4.6 ms and rapid-scan experiments from 4.3 ms to 3.9 s. The difference spectra from 1 μs onward were concatenated and analyzed by a global multiexponential fit using a kinetic model of sequential first-order reactions with four intermediates. The fit yielded lifetimes of the intermediates I_1', I_1, I_2, and I_3 of τ_1' = 51 μs, τ_1 = 290 μs, τ_2 = 29 ms, and τ_3 = 3.3 s, respectively. The resulting concentration profiles were used to calculate the species-associated difference spectra (SADS). SADS and concentration profiles (Figures S2 and S3, Supporting Information) were multiplied to obtain a fitted data set for illustration (Figure 3A). The SADS obtained from the model of sequential first-order reactions exhibit a decrease in the yield from I_1 to I_3, indicating their partial relaxation to the dark state. Therefore, back reactions from I_1 and I_2 to the dark state need to be included in the kinetic model to provide for additional decay pathways (Scheme 1) (Figure S4, Supporting Information). Thus, I_1 and I_2 each exhibit two decay channels with the apparent rate constants $k_1 = k_{f,1} + k_{b,1} = (290\ \mu s)^{-1}$ and $k_2 = k_{f,2} + k_{b,2} = (29\ ms)^{-1}$, respectively. A nonlinear fit using this model yielded rate constants of $k_{f,1} = (500\ \mu s)^{-1}$ and $k_{b,1} = (690\ \mu s)^{-1}$ for I_1, and $k_{f,2} = (33\ ms)^{-1}$ and $k_{b,2} = (270\ ms)^{-1}$ for I_2. The resulting SADS of I_1, I_2, and I_3 are shown in Figure 3B.

The SADS of I_1' is similar to that of I_1. The only difference is that the SADS of I_1' exhibits broad negative contributions at around 1560 and 1700 cm^{-1} (Figure S3, Supporting Information). The bandwidth of this contribution is far too

DOI: 10.1021/jacs.5b01404
J. Am. Chem. Soc. 2015, 137, 5990−5999

Scheme 1. Kinetic Model Used for the Analysis of the FT-IR Dataset from 1 μs to 3.9 s

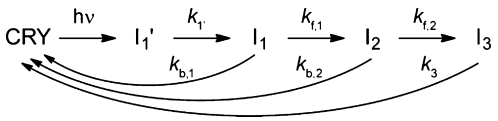

high for an assignment to specific molecular modes, which indicates that I_1' contains some heat artifact caused by the laser irradiation. Its time dependence is very similar to that of the heat relaxation in bacteriorhodopsin films.[43] Therefore, I_1' is not considered to be a separate species and was omitted in the following analysis.

All intermediates show the characteristic band pattern of FADH$^\bullet$ with bands at 1641, 1625, 1611, and 1530 cm^{-1}. Another distinct positive band is found at 1667−1671 cm^{-1}, which has been ascribed to an amide I mode of a turn element.[25] The intensity of this band remains essentially constant throughout the SADS, suggesting a homogeneous decay together with the FADH$^\bullet$ and with the recovery of protonated D396 as observed at 1733 cm^{-1}. The band shift from 1667 to 1671 cm^{-1} in I_3 might lead to a compensation and to the decreased intensity of the negative flavin C═O band at 1693 cm^{-1}.

In I_1, the prominent appearance of the 1641 cm^{-1} band is striking with the adjacent shoulder at 1649 cm^{-1}, which becomes the band maximum in I_3. The band intensity at 1641 cm^{-1} decreases significantly from I_1 to the later intermediates. These observations imply that the 1641/1649 cm^{-1} band does not exclusively originate from a C═O vibration of flavin, but contains an additional contribution from an amide I band of helical elements.[44]

Aside from the positive difference bands, distinct negative contributions are observed, too, which change drastically in the scaled comparison and therefore do not originate from oxidized flavin but rather from either changes in secondary structure or specific amino acids. The most noticeable features in the frequency region of amide I and amide II are found at 1693, 1632, and 1545 cm^{-1}, all occurring in the SADS of I_2. The 1632 cm^{-1} band has previously been reported for steady-state light-*minus*-dark spectra of CPH1-PHR and has been preliminarily assigned to an amide I mode of the protein moiety.[25] Judging from the transition from I_1 to I_2, the band seems to become so strong that it significantly reduces the intensity of the two prominent, adjacent bands.

As for its assignment to specific secondary structure elements, the frequency ranges 1641−1623 cm^{-1} (average 1633 cm^{-1}) and 1695−1674 cm^{-1} (average 1684 cm^{-1}) have unanimously been associated with β-sheets in the literature,[44] whereas the frequency of 1545 cm^{-1} is typical of a less specific amide II contribution. In a more recent FT-IR study of a 50-protein database built for secondary structure prediction,[36] maximum associations with β-sheets were observed for the frequencies 1691 and 1634 cm^{-1}, i.e., these frequencies predicted the occurrence of β-sheets in proteins best. Hence, the marked negative contributions at these very specific positions in the SADS of I_2 are interpreted as evidence for a significant loss of β-sheet structure in this intermediate. Of note, these features are lost in the following intermediate I_3.

To illustrate the rise and decay of the change in β-sheet structure, associated band kinetics are compared to those of other contributions. First, the negative marker band of FAD_{ox} at

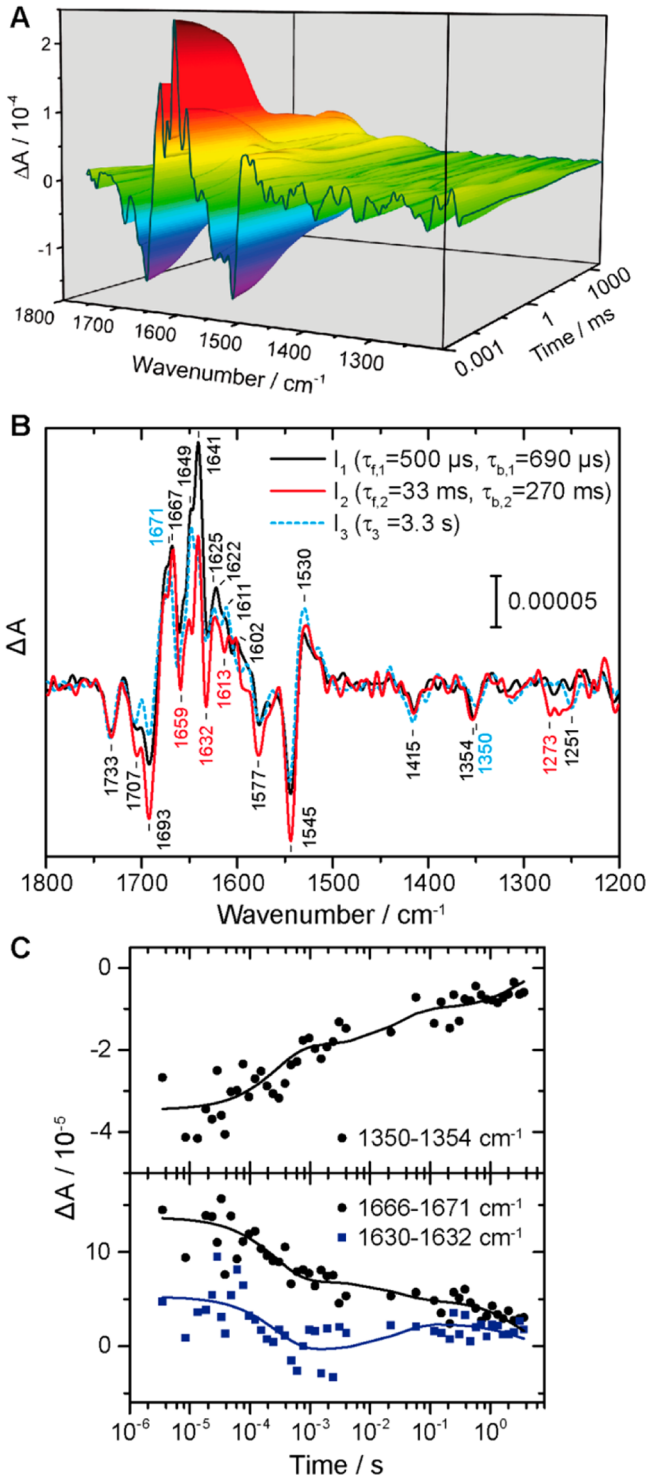

Figure 3. Results of the global fit of the time-resolved FT-IR data set of CPH1-PHR. (A) Three-dimensional representation of the fitted difference spectra with a logarithmic time scale (3.5 μs to 3.63 s). (B) Species-associated difference spectra of the intermediates I_1−I_3. I_2 is characterized by a pronounced loss of β-sheet content, as deduced from the typical bands at 1693, 1632, and 1545 cm^{-1}. (C) Development of selected marker bands over time and respective global fit. The band at 1350−1354 cm^{-1} shows the recovery of the oxidized state of FAD. The positive band assigned to turn elements at 1666−1671 cm^{-1} decays monotonously, whereas the negative band at 1630−1632 cm^{-1} that represents the loss of β-sheet structure reaches a local extremum at ∼1 ms.

DOI: 10.1021/jacs.5b01404
J. Am. Chem. Soc. 2015, 137, 5990−5999

1350−1354 cm^{-1} shows a monotonous decay, indicating the recovery of FAD_{ox} from $FADH^{\bullet}$ (Figure 3C). In parallel with this back reaction, the positive band of turn elements at 1666−1671 cm^{-1} also decays monotonously (Figure 3C), whereas the negative band at 1630−1632 cm^{-1} of β-sheet structure becomes more pronounced and reaches a local extremum in the early millisecond time range. It then starts to decay again, remaining almost constant in the later millisecond to second time range. Consequently, changes in turn elements and β-sheet structure exhibit completely different kinetics. The increase in turn elements is already fully developed at the earliest observation of $FADH^{\bullet}$ at 3.5 μs and decays completely afterward in parallel with the recovery of FAD_{ox}. By contrast, the loss of β-sheet rises together with I_2 much later in the submillisecond region and decays again within tens of milliseconds, and is thus not related to the kinetics of the chromophore.

In summary, three distinct intermediates were identified in the time-resolved data set. The most noticeable feature in the SADS is a conformational change identified as a loss of β-sheet structure. This change occurs in the second intermediate I_2, which rises and decays with time constants of 500 μs and 29 ms, respectively, and differs significantly from the kinetics of changes in turn elements.

Kinetics of Tryptophan and Tyrosine Radicals. Previous time-resolved UV−vis experiments showed the formation of tryptophan and tyrosine radicals in the photoreactions of CPH1 and *At*Cry1.[20−23] $Trp^{\bullet}$ is formed by ultrafast electron transfer to the flavin and deprotonation in the picosecond and nanosecond time regions.[22,23] $Trp^{\bullet}$ appears to decay into a tyrosine radical $TyrO^{\bullet}$ with a half-life of ∼1 ms as demonstrated for *At*Cry1.[21] For CPH1-PHR, evidence for the formation of $TyrO^{\bullet}$ is missing.

Time-resolved UV−vis difference spectra of CPH1-PHR were recorded in the time range of 17 μs to 5 s (Figure S5, Supporting Information). Both $Trp^{\bullet}$ and $TyrO^{\bullet}$ are readily accessible via UV−vis spectroscopy and exhibit distinct band patterns. The $Trp^{\bullet}$ *minus* TrpH difference spectrum exhibits a very broad band centered at around 510 nm,[45] whereas the $TyrO^{\bullet}$ *minus* TyrOH spectrum was determined in water to contain two sharp, adjacent bands at 388 and 408 nm (Figure 4A), in agreement with previous recordings at 140 K.[46] Additionally, protein-bound $FADH^{\bullet}$ *minus* FAD_{ox} shows a characteristic positive contribution in the 500−600 nm region. All these three reference spectra were necessary to fully reconstruct the time-resolved spectra of CPH1-PHR. For each time-resolved spectrum, the amount of $FADH^{\bullet}$, $Trp^{\bullet}$, and $TyrO^{\bullet}$ was varied in order to obtain the best match between the recorded spectrum and the fitted sum spectrum (Figure 4A). The fractions were transformed into molar concentrations using the absorption coefficients of the species.

The resulting kinetics of $FADH^{\bullet}$ was fitted using the time constants (τ_1 = 290 μs, τ_2 = 29 ms) obtained from the global fit of the FT-IR data set (Figure 4B). The agreement of the fit with the experimental data supports the proposed kinetic model with back reactions (Scheme 1) and points to a similar behavior of CPH1-PHR under the conditions of the FT-IR and UV−vis experiments. The decay kinetics of $Trp^{\bullet}$ can be fitted well by a single monoexponential function (Figure 4C). By contrast, the concentration of $TyrO^{\bullet}$ rises to a maximum at ∼1 ms before decaying completely. The simplest kinetic model for this pathway can be formulated as a decay of $Trp^{\bullet}$ into $TyrO^{\bullet}$ with a rate constant k_1 and a consecutive decay of $TyrO^{\bullet}$ with a rate constant k_2. A global fit with shared parameters yielded

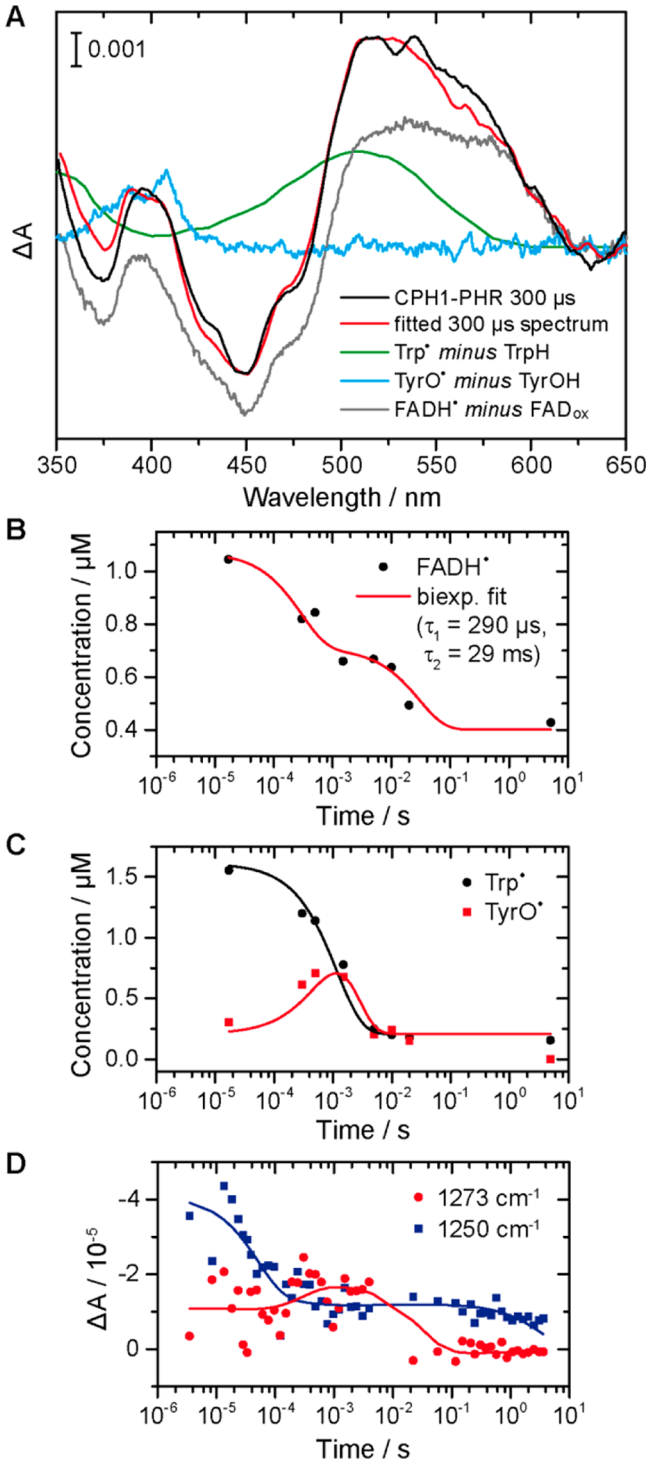

Figure 4. Kinetics of flavin, tryptophan and tyrosine radicals in CPH1-PHR by time-resolved UV−vis spectroscopy. (A) Difference spectrum at 300 μs after the laser pulse and a fitted sum spectrum of contributions by $FADH^{\bullet}$, $Trp^{\bullet}$, and $TyrO^{\bullet}$. (B) Plot of the concentration of $FADH^{\bullet}$ against time as determined from the UV−vis experiments, and fit using the time constants from the global fit of the FT-IR data set. (C) Plot of the concentrations of $Trp^{\bullet}$ and $TyrO^{\bullet}$, and their mono- and biexponential fits, respectively. (D) Kinetics of the negative FT-IR bands at 1273 and 1250 cm^{-1} and global fit of these bands. The band at 1250 cm^{-1} indicates a monotonous recovery of oxidized FAD, whereas the band at 1273 cm^{-1} shows a local extremum at around 1 ms, similar to the kinetics of $TyrO^{\bullet}$ in the UV−vis range in (C). Therefore, the 1273 cm^{-1} band is assigned to a tyrosine residue.

DOI: 10.1021/jacs.5b01404
J. Am. Chem. Soc. 2015, 137, 5990−5999

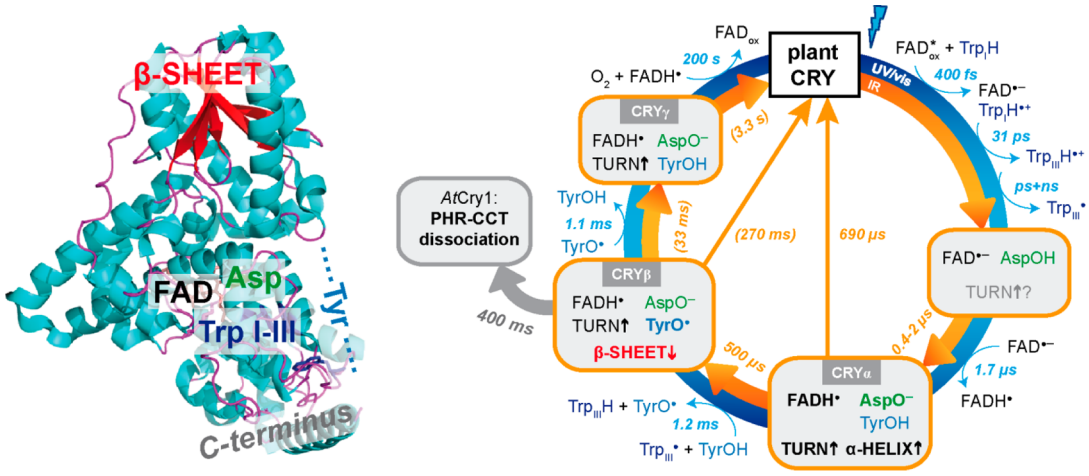

Figure 5. Proposed photocycle for plant cryptochromes including the intermediates CRYα (I_1), CRYβ (I_2), and CRYγ (I_3), on the basis of time-resolved FT-IR spectroscopy (orange) on CPH1-PHR (this work) as well as present and previous time-resolved UV–vis spectroscopy (blue) on CPH1-PHR,[20,22,37] and transient grating spectroscopy (gray) on *At*Cry1.[32] The structure on the left represents the PHR of *At*Cry1 (PDB code: 1U3C). The location of FAD and important amino acids in the α-helical subdomain as well as the only β-sheet of the PHR within the α/β subdomain are highlighted. The lifetimes of CRYβ and CRYγ have to be considered preliminary because of the acceleration of the back reaction by ferricyanide, and have therefore been set in brackets.

lifetimes of τ_1 = (1.2 ± 0.2) ms and τ_2 = (1.1 ± 0.4) ms. Deviations of fitted curves from experimental data that are evident in the kinetics of TyrO$^•$ might be explained by deviations in the reported absorption coefficients of Trp$^•$ and TyrO$^•$ as well as by inaccuracies in the concentration fractions of the species as obtained by the spectral fit. The determined lifetime of Trp$^•$ of τ_1 = 1.2 ms is in good agreement with a reported half-life of $t_{1/2} \approx 1$ ms ($\tau \approx 1.4$ ms) for the conversion of Trp$^•$ into TyrO$^•$ in *At*Cry1.[21] In contrast to *At*Cry1, however, TyrO$^•$ exhibits a faster decay of τ_2 = 1.1 ms as compared to ~7.2 ms in *At*Cry1, and there is no indication of a significant contribution from a slower decay with $t_{1/2}$ >100 ms. Instead, both radicals seem to decay with almost the same lifetime of ~1 ms in CPH1-PHR.

In contrast to the UV–vis spectral range, the absorption of Trp$^•$ and TyrO$^•$ in the infrared remains mostly elusive because of the small absorption coefficients and a lack of reference spectra. Negative difference bands from the reduced amino acids in the dark state may be identifiable, though. Indeed, the SADS of I_2 contains a pronounced negative band at 1273 cm^{-1}, which is not present to this extent in the other intermediates (Figure 3B). This band may be assigned to the characteristic tyrosine band at 1235–1270 cm^{-1}, which originates from CO and CC stretching vibrations of the tyrosyl residue.[44] The difference absorbance at 1273 cm^{-1} (Figure 4D) shows essentially the same kinetic profile as TyrO$^•$ in the UV–vis data set (Figure 4C). It also rises to a maximum at ~1 ms and decays completely within ~20 ms. The global fit of this band suggests a slower decay as compared to the UV–vis, but this deviation can be attributed to the few experimental data points between 5 and 20 ms. The fact that this band occurs at the very end of its reported frequency range of 1235–1270 cm^{-1} is indicative of a tyrosine that acts as a strong hydrogen bond donor via its phenolic OH group.[47−49] As a control, the ΔA values of the adjacent band at 1250 cm^{-1} were analyzed (Figure 4D). These values show a monotonous decay similar to those of other flavin bands. This finding supports the assignment of the 1273 cm^{-1} band to a tyrosine residue and argues against an involvement of other less hydrogen-bonded tyrosine residues absorbing at around 1250 cm^{-1}. The identity of the tyrosine remains to be elucidated because of the unresolved ambiguity in the assignment of the terminal tryptophan in cryptochromes by EPR,[50] transient grating,[32] and UV–vis spectroscopy.[22,51] It has been demonstrated that taking the distances as the only criterion for the assignment of the electron transfer pathway may be misleading.[50]

In summary, the time-resolved UV–vis data show the formation of TyrO$^•$ from Trp$^•$ within ~1 ms and its decay on the same time scale. Complementary FT-IR data imply that the tyrosine residue in question acts as a strong hydrogen bond donor in its reduced state.

DISCUSSION

Time-resolved infrared spectroscopy on plant cryptochrome demonstrated the presence of FAD$^{•-}$ at 500 ns after the laser pulse. FADH$^•$ was subsequently formed concomitant with the deprotonation of D396. In the late microsecond region, major structural changes were observed, which were identified as a loss of β-sheet content. These findings have been integrated into a photocycle for plant cryptochromes (Figure 5) and will be discussed below with a focus on the proton transfer and on the potential role of the β-sheet unfolding for the signal propagation in these light receptors.

Protonation of FAD$^{•-}$ and Comparison to Theory. Time-resolved UV–vis spectroscopy on CPH1-PHR and *At*Cry1 showed the formation of FADH$^•$ from FAD$^{•-}$ on a time scale of a few microseconds.[15,20] This assignment was challenged by recent theoretical studies applying ab initio quantum chemical methods and molecular dynamics (MD) simulations on a model of the active site of *At*Cry1.[30,31] It was demonstrated that protonation of FAD$^{•-}$ is indeed energetically favorable. However, according to the derived model, FAD$^{•-}$ becomes protonated by the W400 cation radical very early on the nanosecond time scale mediated by a protonated D396. In a subsequent step in the nanosecond to microsecond time region, the W377 → W400$^•$ electron transfer within the triad takes place presumably together with a proton transfer from D396 to W400$^•$.

DOI: 10.1021/jacs.5b01404
J. Am. Chem. Soc. 2015, 137, 5990–5999

In contrast, the evolution of anisotropy in ultrafast UV−vis experiments on CPH1-PHR indicated that electron transfer within the tryptophan triad occurs on the subnanosecond time scale.[22] In the present study, a lifetime of $FAD^{\bullet-}$ of 0.4−2 μs was determined by time-resolved FT-IR spectroscopy (Figure 2). The infrared signature of $FAD^{\bullet-}$ was separated from that of the concomitant species $FADH^{\bullet}$ and could be unambiguously assigned using the spectrum of the CPH1-D396C mutant. More importantly, the bleaching of the CO stretching vibration of the proton donor D396 was observed to be directly linked to the $FAD^{\bullet-} \rightarrow FADH^{\bullet}$ transition. The corresponding band at ~1730 cm^{-1} is only weakly developed at 500 ns but reaches its full extent in the subsequent spectrum at 3.5 μs. D396 then remains deprotonated for the whole experimental time window and is finally reprotonated concomitant with flavin reoxidation. We cannot exclude that a minority of $FADH^{\bullet}$ is formed via an ultrafast channel, as pointed out recently,[23] because of the limited time resolution. However, it should be noted that our study is a clear extension to previous findings insofar as we directly monitored the protonation state of D396.

In conclusion, the photoreaction model postulated by Solov'yov et al.[30,31] fails to explain experimental findings in plant cryptochromes, especially concerning the role of D396. Contrary to this model, the time-resolved FT-IR data corroborate the notion of a distinct temporal separation of electron and proton transfer to flavin. Thus, the reorientation of D396 toward the flavin, which is prerequisite for a D396 → $FAD^{\bullet-}$ proton transfer, is likely to occur in the submicrosecond time region rather than within 1 ns. In a recent multiscale computational approach, the inclusion of the nuclear dynamics in the environment of the active site led to a much better agreement of electron transfer rates with the experiment.[52] In contrast, the free energy barrier of ΔG = 7.5 kcal/mol as determined for the proton transfer remains too low to account for the observed microsecond process.[52] The delay of the proton transfer has been proposed to be caused by a necessary movement of the α15 helix,[25] which is in a hydrogen-bonding distance to D396 via M381.[27] In contrast, molecular dynamics simulations show a direct hydrogen bond between flavin and protonated D396 in the dark in 70% of the simulation time in absence of ATP, which is similar to our experimental conditions.[53] Evidently, more extensive theoretical and experimental studies are required to elucidate the structural aspects and concomitant activation barriers of the proton transfer in plant cryptochrome.

Location and Possible Role of Conformational Changes. The global fit of the time-resolved FT-IR data set yielded three separate intermediates I_1 to I_3, which are characterized by an increase in α-helices (I_1), and by a loss of β-sheet (I_2), respectively. I_3 essentially only represents the recovery of the protein into the dark state. As a consistent notation for the reaction intermediates in cryptochromes is not yet available, the intermediates I_1, I_2, and I_3 will be referred to as CRYα, CRYβ, and CRYγ henceforth, in analogy to the major structural changes in I_1 and I_2.

The loss of β-sheet structure in CRYβ rises with a time constant of 500 μs and decays concomitantly with the formation of CRYγ with an apparent time constant of 29 ms, as can be deduced from the corresponding negative marker bands at 1693, 1632, and 1545 cm^{-1} (Figure 3B). The kinetics of the 1632 cm^{-1} band shows that the loss of β-sheet structure becomes maximal at around 1 ms (Figure 3C). The detection of a change in β-sheet structure raises the question as to where this secondary structure element is located in the protein. It can be deduced from the characteristic fold of the PHRs of the photolyase/cryptochrome family that the only candidate for the β-sheet is located in the N-terminal α/β subdomain with its Rossmann-like fold that contains a five-stranded parallel β-sheet. In the crystal structure of *At*Cry1-PHR,[27] the α/β subdomain comprises residues 13−139, whereas the residues 217−495 form the purely α-helical subdomain binding the FAD. The α/β subdomain has not previously been considered to be involved either in the signaling process of sensory cryptochromes or in the photorepair of DNA by photolyases. Its commonly assigned role has been limited to providing a scaffold for the antenna molecule, which is to current knowledge much less tightly bound in sensory cryptochromes than in photolyases.[27] The latter finding is in line with the fact that plant cryptochromes can act as efficient light sensors without an antenna molecule,[23] considering the sufficiently high absorption coefficient of the oxidized flavin. Therefore, the reason for the high conservation of this α/β subdomain in sensory cryptochromes is unclear.

The function of this β-sheet and its unfolding in the signaling process is not directly evident, considering that the signaling is effected by the CCT.[3] CCTs show robust binding to the cognate PHRs and seem to undergo a folded/unfolded transition upon light excitation of the PHR.[32,33] The unfolded part of the CCT may then be ready to interact with downstream signaling partners. On the basis of our results, we reason that the β-sheet of the PHR α/β subdomain may play a central role in the interaction between PHR and CCT. The α/β subdomain of *At*Cry1 exhibits a positively charged surface patch in the region around the α1 helix, β5 strand, and α5 helix, which may provide an interaction site for the largely acidic CCT (Figures S6 and S7, Supporting Information). This charge distribution is conserved in PHR and CCT of CPH1 but not in PHR and CCT of mouse cryptochrome 1[54] in agreement with the light-independent function of the latter protein (Figure S6, Supporting Information). Other charged surface regions of the mouse cryptochrome 1-PHR have been shown to be involved in the binding of the clock protein PERIOD 2.[54] In plant cryptochromes, the C-terminal part of the CCT is considered to be long enough to extend to the α/β subdomain of the PHR (Figure 5). Consistent with this structural model, the C-terminal part of the CCT is particularly sensitive to light-induced trypsin digestion and is therefore likely to undergo the largest structural changes, whereas the N-terminal part seems to be tightly bound to the PHR.[33] In contrast, the CCT of *Drosophila* cryptochrome comprises only few residues and directly binds to the α-helical subdomain close to the FAD binding pocket.[54,55] The relative orientation of the CCT and the exact nature of the PHR-CCT interaction in plant cryptochromes are unclear because a crystal structure of the full-length receptor is not available. We postulate that the β-sheet provides a scaffold for proximal, charged PHR-CCT interaction sites on the protein surface. Then, the light-induced β-sheet unfolding may represent a key step in the dissociation of the PHR-CCT complex and the subsequent unfolding of the CCT.

Rise and Decay of Conformational Changes. When considering the time scales of the aforementioned processes, the β-sheet unfolding in CPH1-PHR was found to proceed on a submillisecond time scale with τ = 500 μs, whereas the unfolding of the CCT in *At*Cry1 was reported to occur in the late millisecond time region with τ = 400 ms.[32] The time

DOI: 10.1021/jacs.5b01404
J. Am. Chem. Soc. 2015, 137, 5990−5999

constants of these processes are consistent with a photoreaction model in which (a) the molecular changes induced by the photoexcitation of FAD have to migrate within hundreds of microseconds from the flavin chromophore to the *secondary structure* element, the β-sheet, located at a distance of ~25 Å, and in which (b) resulting changes in the *tertiary structure* proceed much later within hundreds of milliseconds because of the time-consuming dissociation and unfolding of large parts of the CCT.

In CPH1-PHR, the conformational changes revert together with the decay of the tyrosine radical by formation of the final intermediate CRYγ. Of note, the lifetimes of CRYβ and CRYγ with τ = 29 ms and τ = 3.3 s, respectively, are very likely strongly dependent on the concentration of the oxidant ferricyanide in the protein solution, which was necessary to achieve a suitable repetition rate for the experiment. Without this oxidant, $FADH^{\bullet}$ is reoxidized by oxygen with a time constant of ~200 s.[37] The ferricyanide ions are expected to diffuse into the flavin binding pocket and oxidize the neutral radical on a millisecond time scale. Hence, in the absence of ferricyanide, the decay of CRYβ and the formation of CRYγ might be delayed into the seconds to minutes time range. In contrast, CRYβ formation in the submillisecond time range does not seem to be affected by the addition of oxidants, which is demonstrated by the good agreement between the kinetics of tyrosine conversion in the infrared and UV−vis spectral range, as determined with and without ferricyanide, respectively (Figures 4C and D).

From these considerations it follows that steady-state FT-IR difference spectra recorded without ferricyanide over a period of a few minutes might represent a mixture of CRYβ and CRYγ. Indeed, the comparison between the steady-state difference spectrum and the SADS of CRYβ and CRYγ shows that the loss of β-sheet as the characteristic feature of CRYβ is still pronounced in the steady-state spectrum (Figure S8, Supporting Information). Therefore, the conformational changes in the β-sheet seem to be persistent enough to maintain the rupture of the PHR-CCT interface on a time scale of a few minutes, which represents the relevant time scale for the lifetime of the signaling state $FADH^{\bullet}$ in vivo.[19]

CONCLUSIONS

Time-resolved infrared spectroscopy on a plant cryptochrome PHR enabled us (a) to detect the deprotonation of the proton donor D396 concomitantly with the microsecond protonation of $FAD^{\bullet-}$, and (b) to reveal the submillisecond unfolding of a β-sheet element in the PHR and specifically trace it to the α/β subdomain. This subdomain has previously not been considered to be involved in the signaling of sensory cryptochromes despite its evolutionary conservation. Interestingly, in the nonsensory mouse cryptochrome 1, the point mutation R109Q within the α/β subdomain leads to disruption of its binding to other core components of the clock, BMAL1 and CLOCK.[56] The role of the α/β subdomain might therefore have changed in both plant and mammalian cryptochromes, away from antenna binding.

We infer from our findings that the unfolding event in the α/β subdomain may constitute a key step in the initiation of the signaling cascade in plant cryptochromes by enabling the subsequent dissociation of the PHR-CCT complex. This emerging view of the signal progression resembles an activation via a protein quake as it has been coined for the photoactive yellow protein (PYP).[57] Such a quake would be opposed to a model in which a succession of redox reactions finally activates a signaling partner.[58] As in PYP, the protein quake might originate from the generation of a charge, either of $FAD^{\bullet-}$ or of the deprotonated D396. A prominent role of charges in the signaling process has been suggested for plant cryptochromes in a recent hypothesis.[59] Moreover, the formation of $FAD^{\bullet-}$ has already been demonstrated to be sufficient for the stimulation of a response in the protein conformation of PHR.[24] The specific interaction sites between PHR and CCT of plant cryptochromes remain yet to be identified. This study will motivate an extension of the focus of this search to the α/β subdomain remote from the flavin chromophore.

ASSOCIATED CONTENT

Supporting Information

Experimental section, simulation of spectra for partial radical conversion, concentration profiles and SADS of the intermediates from the global fit using a model of sequential reactions, concentration profiles using a model of sequential reactions with additional back reactions to the dark state, time-resolved UV−vis difference spectra, electrostatic surface potentials of PHRs, sequences of CCTs, and comparison of the steady-state FT-IR difference spectrum with the SADS of CRYβ (I_2) and CRYγ (I_3). The Supporting Information is available free of charge on the ACS Publications website at DOI: 10.1021/jacs.5b01404.

AUTHOR INFORMATION

Corresponding Author

*tilman.kottke@uni-bielefeld.de

Notes

The authors declare no competing financial interest.

ACKNOWLEDGMENTS

We thank Thomas Hellweg for generous support and Ina Ehring for excellent technical assistance. This work was supported by the Deutsche Forschungsgemeinschaft (KO3580/2-1 and KO3580/4-1).

REFERENCES

(1) Chaves, I.; Pokorny, R.; Byrdin, M.; Hoang, N.; Ritz, T.; Brettel, K.; Essen, L. O.; van der Horst, G. T.; Batschauer, A.; Ahmad, M. *Annu. Rev. Plant Biol.* **2011**, *62*, 335−364.
(2) Sancar, A. *J. Biol. Chem.* **2008**, *283*, 32153−32157.
(3) Yang, H. Q.; Wu, Y. J.; Tang, R. H.; Liu, D.; Liu, Y.; Cashmore, A. R. *Cell* **2000**, *103*, 815−827.
(4) Yu, X.; Shalitin, D.; Liu, X.; Maymon, M.; Klejnot, J.; Yang, H.; Lopez, J.; Zhao, X.; Bendehakkalu, K. T.; Lin, C. *Proc. Natl. Acad. Sci. U. S. A.* **2007**, *104*, 7289−7294.
(5) Cashmore, A. R.; Jarillo, J. A.; Wu, Y. J.; Liu, D. *Science* **1999**, *284*, 760−765.
(6) Lin, C.; Shalitin, D. *Annu. Rev. Plant Biol.* **2003**, *54*, 469−496.
(7) Somers, D. E.; Devlin, P. F.; Kay, S. A. *Science* **1998**, *282*, 1488−1490.
(8) Stanewsky, R.; Kaneko, M.; Emery, P.; Beretta, B.; Wager-Smith, K.; Kay, S. A.; Rosbash, M.; Hall, J. C. *Cell* **1998**, *95*, 681−692.
(9) Coesel, S.; Mangogna, M.; Ishikawa, T.; Heijde, M.; Rogato, A.; Finazzi, G.; Todo, T.; Bowler, C.; Falciatore, A. *EMBO Rep.* **2009**, *10*, 655−661.
(10) Beel, B.; Prager, K.; Spexard, M.; Sasso, S.; Weiss, D.; Müller, N.; Heinnickel, M.; Dewez, D.; Ikoma, D.; Grossman, A. R.; Kottke, T.; Mittag, M. *Plant Cell* **2012**, *24*, 2992−3008.

DOI: 10.1021/jacs.5b01404
J. Am. Chem. Soc. 2015, 137, 5990−5999

(11) Hendrischk, A. K.; Frühwirth, S. W.; Moldt, J.; Pokorny, R.; Metz, S.; Kaiser, G.; Jäger, A.; Batschauer, A.; Klug, G. *Mol. Microbiol.* **2009**, *74*, 990−1003.
(12) Zhu, H.; Sauman, I.; Yuan, Q.; Casselman, A.; Emery-Le, M.; Emery, P.; Reppert, S. M. *PLoS Biol.* **2008**, *6*, e4.
(13) Griffin, E. A., Jr.; Staknis, D.; Weitz, C. J. *Science* **1999**, *286*, 768−771.
(14) Gegear, R. J.; Casselman, A.; Waddell, S.; Reppert, S. M. *Nature* **2008**, *454*, 1014−1018.
(15) Maeda, K.; Robinson, A. J.; Henbest, K. B.; Hogben, H. J.; Biskup, T.; Ahmad, M.; Schleicher, E.; Weber, S.; Timmel, C. R.; Hore, P. J. *Proc. Natl. Acad. Sci. U. S. A.* **2012**, *109*, 4774−4779.
(16) Ritz, T.; Adem, S.; Schulten, K. *Biophys. J.* **2000**, *78*, 707−718.
(17) Banerjee, R.; Schleicher, E.; Meier, S.; Viana, R. M.; Pokorny, R.; Ahmad, M.; Bittl, R.; Batschauer, A. *J. Biol. Chem.* **2007**, *282*, 14916−14922.
(18) Bouly, J. P.; Schleicher, E.; Dionisio-Sese, M.; Vandenbussche, F.; Van Der Straeten, D.; Bakrim, N.; Meier, S.; Batschauer, A.; Galland, P.; Bittl, R.; Ahmad, M. *J. Biol. Chem.* **2007**, *282*, 9383−9391.
(19) Herbel, V.; Orth, C.; Wenzel, R.; Ahmad, M.; Bittl, R.; Batschauer, A. *Plant J.* **2013**, *74*, 583−592.
(20) Langenbacher, T.; Immeln, D.; Dick, B.; Kottke, T. *J. Am. Chem. Soc.* **2009**, *131*, 14274−14280.
(21) Giovani, B.; Byrdin, M.; Ahmad, M.; Brettel, K. *Nat. Struct. Biol.* **2003**, *10*, 489−490.
(22) Immeln, D.; Weigel, A.; Kottke, T.; Pérez Lustres, J. L. *J. Am. Chem. Soc.* **2012**, *134*, 12536−12546.
(23) Müller, P.; Bouly, J. P.; Hitomi, K.; Balland, V.; Getzoff, E. D.; Ritz, T.; Brettel, K. *Sci. Rep.* **2014**, *4*, 5175.
(24) Hense, A.; Herman, E.; Oldemeyer, S.; Kottke, T. *J. Biol. Chem.* **2015**, *290*, 1743−1751.
(25) Immeln, D.; Pokorny, R.; Herman, E.; Moldt, J.; Batschauer, A.; Kottke, T. *J. Phys. Chem. B* **2010**, *114*, 17155−17161.
(26) Kottke, T.; Batschauer, A.; Ahmad, M.; Heberle, J. *Biochemistry* **2006**, *45*, 2472−2479.
(27) Brautigam, C. A.; Smith, B. S.; Ma, Z.; Palnitkar, M.; Tomchick, D. R.; Machius, M.; Deisenhofer, J. *Proc. Natl. Acad. Sci. U. S. A.* **2004**, *101*, 12142−12147.
(28) Li, X.; Wang, Q.; Yu, X.; Liu, H.; Yang, H.; Zhao, C.; Liu, X.; Tan, C.; Klejnot, J.; Zhong, D.; Lin, C. *Proc. Natl. Acad. Sci. U. S. A.* **2011**, *108*, 20844−20849.
(29) Engelhard, C.; Wang, X.; Robles, D.; Moldt, J.; Essen, L. O.; Batschauer, A.; Bittl, R.; Ahmad, M. *Plant Cell* **2014**, *26*, 4519−4531.
(30) Solov'yov, I. A.; Domratcheva, T.; Moughal Shahi, A. R.; Schulten, K. *J. Am. Chem. Soc.* **2012**, *134*, 18046−18052.
(31) Solov'yov, I. A.; Domratcheva, T.; Schulten, K. *Sci. Rep.* **2014**, *4*, 3845.
(32) Kondoh, M.; Shiraishi, C.; Müller, P.; Ahmad, M.; Hitomi, K.; Getzoff, E. D.; Terazima, M. *J. Mol. Biol.* **2011**, *413*, 128−137.
(33) Partch, C. L.; Clarkson, M. W.; Özgür, S.; Lee, A. L.; Sancar, A. *Biochemistry* **2005**, *44*, 3795−3805.
(34) Barth, A. *Biochim. Biophys. Acta* **2007**, *1767*, 1073−1101.
(35) Ataka, K.; Kottke, T.; Heberle, J. *Angew. Chem., Int. Ed.* **2010**, *49*, 5416−5424.
(36) Goormaghtigh, E.; Ruysschaert, J. M.; Raussens, V. *Biophys. J.* **2006**, *90*, 2946−2957.
(37) Immeln, D.; Schlesinger, R.; Heberle, J.; Kottke, T. *J. Biol. Chem.* **2007**, *282*, 21720−21728.
(38) Thöing, C.; Pfeifer, A.; Kakorin, S.; Kottke, T. *Phys. Chem. Chem. Phys.* **2013**, *15*, 5916−5926.
(39) Bauer, C.; Rabl, C. R.; Heberle, J.; Kottke, T. *Photochem. Photobiol.* **2011**, *87*, 548−553.
(40) Ataka, K.; Hegemann, P.; Heberle, J. *Biophys. J.* **2003**, *84*, 466−474.
(41) Yamada, D.; Zhang, Y.; Iwata, T.; Hitomi, K.; Getzoff, E. D.; Kandori, H. *Biochemistry* **2012**, *51*, 5774−5783.
(42) Iwata, T.; Zhang, Y.; Hitomi, K.; Getzoff, E. D.; Kandori, H. *Biochemistry* **2010**, *49*, 8882−8891.
(43) Lórenz-Fonfría, V. A.; Furutani, Y.; Kandori, H. *Biochemistry* **2008**, *47*, 4071−4081.
(44) Barth, A.; Zscherp, C. *Q. Rev. Biophys.* **2002**, *35*, 369−430.
(45) Solar, S.; Getoff, N.; Surdhar, P. S.; Armstrong, D. A.; Singh, A. *J. Phys. Chem.* **1991**, *95*, 3639−3643.
(46) Proshlyakov, D. A. *Biochim. Biophys. Acta* **2004**, *1655*, 282−289.
(47) Hienerwadel, R.; Boussac, A.; Breton, J.; Diner, B. A.; Berthomieu, C. *Biochemistry* **1997**, *36*, 14712−14723.
(48) Iwata, T.; Watanabe, A.; Iseki, M.; Watanabe, M.; Kandori, H. *J. Phys. Chem. Lett.* **2011**, *2*, 1015−1019.
(49) Takahashi, R.; Okajima, K.; Suzuki, H.; Nakamura, H.; Ikeuchi, M.; Noguchi, T. *Biochemistry* **2007**, *46*, 6459−6467.
(50) Biskup, T.; Hitomi, K.; Getzoff, E. D.; Krapf, S.; Koslowski, T.; Schleicher, E.; Weber, S. *Angew. Chem., Int. Ed.* **2011**, *50*, 12647−12651.
(51) Zeugner, A.; Byrdin, M.; Bouly, J. P.; Bakrim, N.; Giovani, B.; Brettel, K.; Ahmad, M. *J. Biol. Chem.* **2005**, *280*, 19437−19440.
(52) Lüdemann, G.; Solov'yov, I. A.; Kubar, T.; Elstner, M. *J. Am. Chem. Soc.* **2015**, *137*, 1147−1156.
(53) Cailliez, F.; Müller, P.; Gallois, M.; de la Lande, A. *J. Am. Chem. Soc.* **2014**, *136*, 12974−12986.
(54) Czarna, A.; Berndt, A.; Singh, H. R.; Grudziecki, A.; Ladurner, A. G.; Timinszky, G.; Kramer, A.; Wolf, E. *Cell* **2013**, *153*, 1394−1405.
(55) Zoltowski, B. D.; Vaidya, A. T.; Top, D.; Widom, J.; Young, M. W.; Crane, B. R. *Nature* **2011**, *480*, 396−399.
(56) Nangle, S. N.; Rosensweig, C.; Koike, N.; Tei, H.; Takahashi, J. S.; Green, C. B.; Zheng, N. *eLife* **2014**, *3*, e03674.
(57) Xie, A.; Kelemen, L.; Hendriks, J.; White, B. J.; Hellingwerf, K. J.; Hoff, W. D. *Biochemistry* **2001**, *40*, 1510−1517.
(58) Öztürk, N.; Song, S. H.; Selby, C. P.; Sancar, A. *J. Biol. Chem.* **2008**, *283*, 3256−3263.
(59) Müller, P.; Bouly, J. P. *FEBS Lett.* **2015**, *589*, 189−192.

DOI: 10.1021/jacs.5b01404
J. Am. Chem. Soc. 2015, 137, 5990−5999